Aerosol and Air Quality Research, 17: 2509–2521, 2017

ISSN: 1680-8584 print / 2071-1409 online
doi: 10.4209/aaqr.2017.05.0159

Thirteen Years of Aerosol Radiative Forcing in Southwestern Iberian Peninsula

Maria A. Obregón[1*], Maria J. Costa[2], Ana M. Silva[2], Antonio Serrano[3]

[1] *Departamento de Física, Instituto de Ciências da Terra, Instituto de Investigação e Formação Avançada, Universidade de Évora, Évora, 7000-671, Portugal*
[2] *Departamento de Física, Instituto de Ciências da Terra, Escola de Ciências e Tecnologia, Universidade de Évora, Évora, 7000-671, Portugal*
[3] *Departamento de Física, Universidad de Extremadura, Badajoz, 06071, Spain*

ABSTRACT

Notable uncertainties in the aerosol impact on the Earth's radiative budget still remain, mainly at local scales. This study aims to accurately quantify the shortwave aerosol radiative forcing (ARF) and its efficiency (ARFE) at Évora (Portugal, Southwestern Europe). This is an interesting region affected by different aerosol types and sources. Towards this goal, ARF and ARFE are calculated for Évora during thirteen years (2003–2015), which is the longest period ever analyzed for this region. For this calculation, the most updated AERONET data have been used to simulate irradiance with the libRadtran code. Thus, 1676 daily values were analyzed, obtaining a mean ARF of –7.4 W m^{-2} at the Earth's surface (SURF) and –1.1 W m^{-2} at the top of the atmosphere (TOA), indicating a cooling of the Earth–atmosphere system. The difference in ARF between TOA and SURF indicates a mean net gain of 6.3 W m^{-2} for the atmosphere. While no ARF seasonal pattern is observed at the TOA, a clear seasonal cycle is detected at the SURF with the most negative values occurring in summer. On the other hand, ARFE shows mean values of –62.7 W m^{-2} τ^{-1} at the SURF and –14.3 W m^{-2} τ^{-1} at the TOA. Results show that ARFE highly depends on the aerosol single scattering albedo, showing opposite behavior at the SURF and at the TOA. The large temporal variability detected in the aerosol properties in the region of study confirms the general need for long time series of measurements to achieve an accurate estimation of the ARF and ARFE.

Keywords: Aerosol radiative effects; Long term analysis; Radiative transfer model; AERONET.

INTRODUCTION

Atmospheric aerosol particles, of natural or anthropogenic origin, interact directly with solar and terrestrial radiation through scattering and absorption as well as through emission processes, modifying the Earth's radiative balance. This effect is quantified by the aerosol radiative forcing (ARF) calculated as the change in the radiative balance due exclusively to the existence of aerosols. According to the Fifth Assessment Report delivered in 2013 by the Intergovernmental Panel on Climate Change, direct and indirect effects of aerosols in the atmosphere result in an overall radiative forcing of –0.9 (–1.9 to –0.1) W m^{-2} at the TOA (Boucher *et al.*, 2013). Although this global cooling effect due to aerosols is well established, significant uncertainties still remain, mainly referred to their spatial and temporal variability at regional and local scales. Thus, due to nearby point sources, the aerosol radiative forcing at the local scale can exceed the global values by an order of magnitude. Additionally, most climate models underestimate the negative radiative forcing caused by anthropogenic aerosols (Hansen *et al.*, 2011). Hence, this short-scale information is essential to achieve an accurate knowledge of the impact of aerosols on climate. It is, therefore, important to quantify the long-term aerosol radiative forcing in different areas worldwide, paying special attention to regions of climatic significance.

Within this framework, the Iberian Peninsula is a particularly interesting region affected by occasional intrusions coming from the largest source of dust worldwide: the Sahara Desert. The frequency of these intrusions is modulated by the annual latitudinal displacement of major semi-permanent pressure systems, showing a typical seasonal pattern (Cachorro *et al.*, 2005; Toledano, 2005; Salgueiro *et al.*, 2014) associated to specific synoptic situations (Rodriguez *et al.*, 2001; Querol *et al.*, 2002; Escudero *et al.*, 2005). In addition to the desert dust intrusions, the Iberian Peninsula is notably affected by other sources of aerosols. In particular, the southwestern interior part of the Iberian Peninsula is also exposed to local continental

* Corresponding author.
Tel.: +351 266740800 ext. 5472
E-mail address: nines@unex.es

aerosols and marine aerosols coming from the Atlantic Ocean (Pereira *et al.*, 2005; Elias *et al.*, 2006; Silva *et al.*, 2006; Pereira *et al.*, 2008; Pereira *et al.*, 2011; Obregón *et al.*, 2012). Additionally, wildfires are an occasional but intense source of aerosols for the area in summer. Due to its exposure to a diversity of local and remote aerosol sources, the Iberian Peninsula is a privileged location for studying the aerosol impact on the radiation balance.

A major research site for aerosols in this area is located in Évora (Portugal), deployed by the Institute of Earth Sciences at the University of Évora, where the AErosol Robotic NETwork (AERONET, http://aeronet.gsfc.nasa.gov) has a monitoring station. This station started to operate in 2003 and, since then, provides radiometric measurements of aerosol properties averaged in the atmospheric column according to AERONET standards and protocols. Notable research has been conducted based on these measurements focusing mainly on obtaining typical values for the physical and optical properties of the aerosols during long periods and specific interesting events (Silva *et al.*, 2003; Obregón *et al.*, 2012), identifying most frequent aerosol types in the area (Elias *et al.*, 2006), and studying their radiative effect (Santos *et al.*, 2008; Mateos *et al.* 2014; Obregón *et al.*, 2015a). However, these latter studies are based on a limited period of time (Santos *et al.*, 2008; Mateos *et al.*, 2014) or focus on specific short events (Obregón *et al.*, 2015a), failing to provide an accurate and complete estimation of the aerosol radiative forcing. Therefore, this study gathers the longest series of aerosol measurements ever used for this area in order to accurately estimate the direct aerosol radiative forcing and its efficiency in the shortwave spectral range. In order to thoroughly analyze the impact of aerosols in the total atmosphere, the aerosol radiative forcing and its efficiency will be calculated at the Earth's surface (SURF) and at the top of the atmosphere (TOA).

The paper is structured as follows: first, a brief description of the study region, instrumentation, measurements and methodology is provided (Section 2), followed by the description of the main results (Section 3), and, finally, the main conclusions (Section 4).

METHODOLOGY

Site Description

The current study is based on aerosol experimental measurements registered at the AERONET site located in the city of Évora (Portugal), in southwestern Iberian Peninsula. Fig. 1 shows the location of this station (38.6°N, 7.9°W, 293 m a.s.l), approximately 100 km eastwards from the Atlantic coast.

Évora shows a mainly continental climate attenuated by the maritime influence of the Atlantic Ocean. This climate is classified as Csa (Mediterranean climates with hot and dry summers) according to Köppen-Geiger types (Köppen, 1936). It features very hot and dry summers with prevailing cloud-free conditions. Very high irradiance values, among

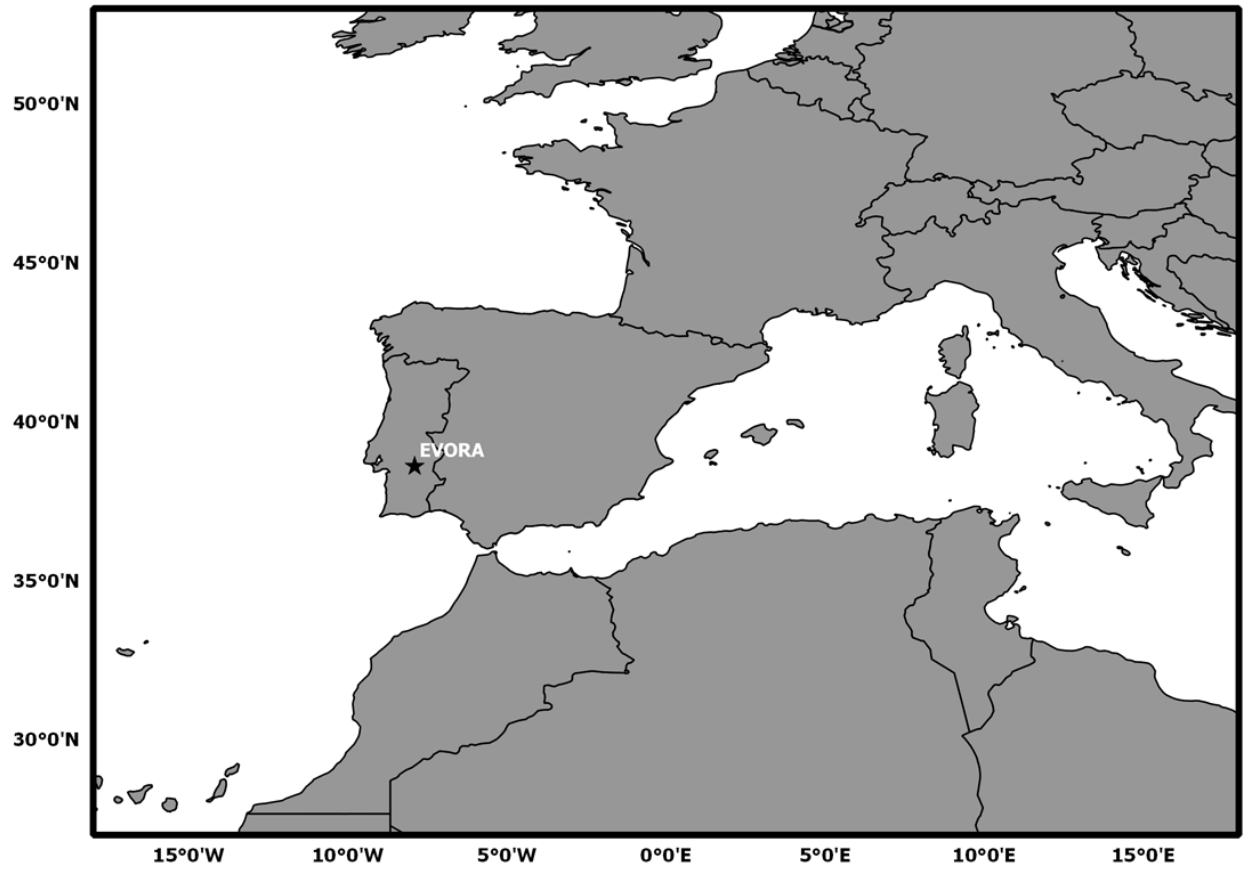

Fig. 1. Location of Évora in the Southwestern Iberian Peninsula.

the highest in Europe, are reached under clear conditions with values up to 1000 W m^{-2} near summer solstice at noon.

Instrumentation

This ground-based station is equipped with a CIMEL CE-318 sunphotometer integrated in the NASA AERONET (Aerosol Robotic NETwork) network (Holben *et al.*, 1998) since 2003. This network provides aerosol information with the aim to establish a ground-based climatology and to identify and characterize the most influential aerosols on the climatic system. The CIMEL CE-318 sunphotometer performs direct sun measurements at 340, 380, 440, 500, 675, 870, 940 and 1020 nm, and measurements of sky radiances in the almucantar and principal plane geometries at 440, 675, 870 and 1020 nm. These measurements are processed following AERONET protocols (Holben *et al.*, 1998) to obtain a variety of aerosol products at different quality levels (1.0, 1.5 and 2.0). The sunphotometer is calibrated annually following AERONET protocols by the AERONET-NASA, RIMA and PHOTONS networks (Holben *et al.*, 1998; Toledano *et al.*, 2006).

Method

It is important to note that the radiative forcing estimates obtained in this study differ from the IPCC definition of radiative forcing. While the IPCC calculates the radiative forcing as the difference between irradiances in the pre-industrial and present day atmosphere due to changes in the concentrations of a certain atmosphere component, in this study, radiative forcing stands for the instantaneous contribution of a particular component (in this case aerosols) to the radiation budget. Thus, it is calculated as the difference in the radiative energy at a given level between a situation where aerosols are present, F, and a situation where these atmospheric particles are absent (background/baseline conditions), F^0:

$$ARF = \left(F_{dn} - F_{up}\right) - \left(F_{dn}^0 - F_{up}^0\right) \quad (1)$$

where F is the flux (shortwave irradiance), the subscript "dn" indicates the downward direction and the subscript "up" the upward direction. In this study, the ARF values calculated at the SURF and at the TOA are analyzed. Thus, radiative forcing can be defined at these two levels as:

$$ARF_{TOA} = F_{up(TOA)}^0 - F_{up(TOA)} \quad (2)$$

$$ARF_{SURF} = \left(1 - A_s\right) \cdot \left(F_{dn(SURF)} - F_{dn(SURF)}^0\right) \quad (3)$$

where A_s is the surface albedo, assumed to be the same for both aerosol situations (background/baseline and presence of aerosols).

To estimate the amount of solar radiations trapped in the atmosphere due to aerosols, the difference in ARF between TOA and SURF is computed. Then, the heating rate (HR) due to aerosol absorption is calculated according to the first law of thermodynamics and assuming hydrostatic equilibrium, as suggested by Liou (2002):

$$\frac{\partial T}{\partial t} = \frac{g}{Cp}\frac{ARF_{ATM}}{\Delta P} \quad (4)$$

where $\partial T/\partial t$ is the HR in K day^{-1}, g is the acceleration due to gravity (9.8 m s^{-2}), Cp is the specific heat capacity of air at constant pressure (i.e., 1006 J kg^{-1} K^{-1}), and ΔP is the atmospheric pressure difference between surface and 3 km altitude, where most aerosols are present. According to several authors, in this study, ΔP was taken as equal to 300 hPa (Kaskaoutis *et al.*, 2013; Singh *et al.*, 2016).

From the ARF instantaneous data, the daily average value (DARF) can be calculated as follows:

$$DARF = \frac{\sum ARF_{hourly}}{24} \quad (5)$$

where ARF_{hourly} are hourly averaged values and the sum extends over the whole day (24 h).

ARF is very sensitive to the amount and type of aerosols existing in the atmosphere, increasing with the AOD. In order to quantify the rate at which the forcing varies per unit optical depth, the aerosol radiative forcing efficiency (ARFE) is defined. The mean ARFE was calculated as the slope of the regression line between ARF and AOD as suggested by Bush and Valero (2003). In this study AOD at 550 nm has been used. The conversion of AOD at 500 nm, which is the AERONET direct product, to AOD at 550 nm has been performed using the Ångstrom power law:

$$AOD550 = AOD500 \cdot \left(\frac{550}{500}\right)^{-\alpha} \quad (6)$$

where α is Ångstrom Exponent in the wavelength range of 440–870 nm (Alam *et al.*, 2011).

The dataset used in this study is composed of cloud-free shortwave irradiance simulated values integrated over the spectral interval 285–2800 nm. The simulations were performed during those days in the period 2003–2015 when level 2.0 AERONET data are available for this station. Thus, 1676 days were used, which is a much higher number than, for example, the 200 days used by Esteve *et al.* (2014). It is important to note that level 2.0 data correspond exclusively to cloud-free conditions.

The shortwave irradiances were simulated using the libRadtran version 1.7 radiative transfer code (Mayer and Kylling, 2005; Emde *et al.*, 2016). The uncertainties of libRadtran model were assessed by Emde *et al.* (2016), who showed that the estimated radiance and irradiance results agree very well with a reference validated model, presenting differences lower than 0.05%, with a few exceptions for cases that are not treated in this work (for example circum-solar radiation). References therein (Emde *et al.*, 2016) to a number of model intercomparison studies demonstrate the performance of libRadtran in comparison to a variety of other models. In addition, Obregón *et al.*

(2015b) analyzed the performance of libRadtran to simulate shortwave solar irradiances under different aerosol conditions, through comparison with corresponding calibrated pyranometer measurements. The authors obtained relative differences between irradiance simulations and measurements lower than 0.2%. Additionally, Román *et al.* (2014) analyzed the sensitivity of SW irradiances simulated with libRadtran model to the input uncertainties, obtaining a global sensitivity usually below 10%.

The main inputs for simulations were aerosol optical properties, precipitable water vapor column, surface albedo, and total ozone column. The inputs to describe the aerosols were provided by AERONET and consist of direct products as aerosol optical depth (AOD) and Ångström parameter, and inversion products as asymmetry parameter (ASY), and single scattering albedo (SSA). Ångström parameters were derived from level 2.0 AERONET aerosol optical depth (AOD) in the range 440–870 nm. Level 2.0 AERONET dataset also provided ASY values. Level 2.0 SSA data are very scarce, with only 226 values available in the period of study. The main reason is the requirement to only consider cases with AOD at 440 nm higher than 0.4. This AOD value is very unusual in Évora (the typical median value is 0.1) and corresponds almost exclusively to desert dust intrusions, which is a very specific situation. Therefore, in order to include different aerosol types and to have enough data available, level 1.5 SSA had to be used. Additionally, data were inspected to search for anomalous values. No negative AOD cases and only eight (0.06% of a total number of cases of 13920) negative Ångström exponent cases were found. The latter were filtered. SSA and ASY values for 675 nm have been used as suggested by some authors (Di Biagio *et al.*, 2010; Foyo-Moreno *et al.*, 2014). This wavelength has been chosen among the wavelengths available at AERONET data as it is close to the maximum of the solar irradiance per unit wavelength. Precipitable water vapor data were also obtained from level 2.0 AERONET products. Daily total ozone column was provided by the AURA Validation Data Center (AVDC) via its website (http://avdc.gsfc.nasa.gov/index.php?site=1593048672&id=28). Surface albedo was obtained from the Surface and Atmospheric Radiation Budget (SARB) working group, part of NASA Langley Research Center's Clouds and the Earth's Radiant Energy System (CERES) mission (http://ceres.larc.nasa.gov/). In order to take into account the time of the year, midlatitude summer/winter standard vertical profiles of thermodynamic variables, main gases and aerosols were considered depending on the season (Shettle *et al.*, 1989; Mayer and Kylling, 2005). The extraterrestrial irradiance was considered according to Gueymard (2004). The radiative transfer equation solver DISORT2, which is an improved version of the multi-stream discrete ordinate method of Stamnes *et al.* (2000), was used with 16 streams.

In order to more accurately model the instantaneous irradiance, 10-minute irradiances were simulated. For this, available AERONET values (α and β Ångström coefficients, ASY, SSA and PWC) were interpolated on a 10-minute basis. The dataset used was composed of 108843 10-minutes values of ARF corresponding to the 1676 days with available AERONET data. Fig. 2 shows the number of days analyzed in this study for each month during the period 2003-2015. Summer is the season with more days with available data (668 days, 40%), due to the prevailing cloud-free conditions during this period of the year. The relative frequency of days with available data for the other seasons was 21% (352 days) in spring, 20% (343 days) in autumn, and 19% (314 days) in winter.

To evaluate the aerosol radiative effects, simulations with and without aerosols were computed for the 108843 cases. Finally, ARF was calculated at the TOA and at the SURF levels, substituting the simulated irradiance in equations 2 and 3, respectively.

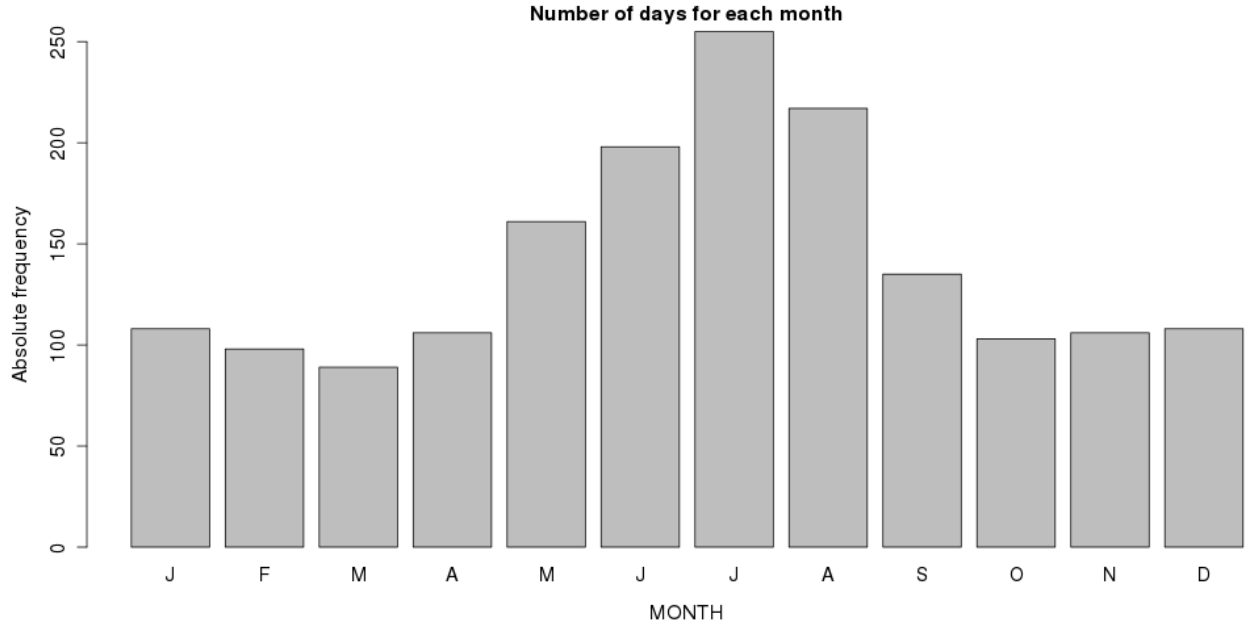

Fig. 2. Number of daily ARF values, DARF, for each month during the period 2003–2015.

The reliability of the libRadtran model for simulating SW irradiance in Évora was previously confirmed by comparing simulated values with irradiance measurements registered by an Eppley Black & White pyranometer (Obregón *et al.*, 2015a). This comparison included clean and turbid cases corresponding to periods before or after (clean), and during (turbid) two particular desert dust intrusion events occurred in summer 2012 (Obregón *et al.*, 2015a). Additionally, in this study the reliability of the libRadtran simulations will be tested by comparing our estimated instantaneous ARF with values provided by AERONET.

RESULTS AND DISCUSSION

Spectral Variation of AOD, SSA and ASY

As mentioned in the methodology, aerosol optical properties such as AOD, SSA and ASY along with their spectral variability are required for calculating ARF and ARFE. These properties have different spectral variations revealing information about the particle size and their absorptivity. Fig. 3 illustrates the AOD, SSA and ASY mean spectral variation for the different seasons.

The spectral variation of AOD provides information about the particle size distribution (Eck *et al.*, 1999). AOD seems to be more wavelength dependent during summer, when it decreases as wavelength increases, indicating the presence of fine particles. Conversely, the smaller spectral dependence is observed in winter, indicating the prevalence of coarser particles. Mean AOD in summer is 0.17 ± 0.12 at 440 nm wavelength and 0.07 ± 0.08 at 1020 nm, whereas, in winter, the mean value is 0.08 ± 0.05 at 440 nm and 0.03 ± 0.02 at 1020 nm.

In regard to SSA, Fig. 3 shows the mean values for each season of the year. As can be seen, mean SSA values for the four seasons decrease as wavelength increases. This SSA spectral behavior indicates the presence of absorbing aerosols (Dubovik *et al.*, 2002). This wavelength dependence is more intense in winter than during the other seasons of the year, with mean values of 0.88 ± 0.08 at 440 nm and 0.80 ± 0.14 at 1020 nm. This dependence is also reported for Lahore and Karachi by Alam *et al.* (2012), Delhi by Singh *et al.* (2010), and four locations in the Indo-Gangetic plains by Bibi *et al.* (2016), but only during winter, when dust is not a major contributor to the aerosol load.

Additionally, the mean value corresponding to AERONET level 2.0 SSA data has been added to Fig. 3(b). In contrast to the behavior found for the SSA data used in this work, level 2.0 SSA presents higher values and increases or is neutral with wavelength, which is a clear signature of the predominance of mineral dust (Dubovik *et al.*, 2002). This fact is due to the extremely restrictive threshold used for level 2.0 data, which requires AOD higher than 0.4. In the case of Évora, this threshold mostly retains those cases with desert dust aerosols originating from the Sahara region. Since this study attempts to analyze the mean aerosol radiative forcing in southwestern Iberian Peninsula during thirteen years, a variety of aerosol conditions needs to be sampled. Therefore, for this study, the level 2.0 AERONET data is too restrictive regarding the SSA.

Similarly to AOD and SSA, ASY shows spectral dependence (Fig. 3(c)). In general ASY decreases with increasing wavelength, except for high wavelengths, where a marginal increase can be observed for spring, summer and autumn seasons. Mean ASY (standard deviation) is 0.70 (0.03) at 440 nm and 0.66 (0.04) at 1020 nm in spring, 0.70 (0.03) at 440 nm and 0.65 (0.05) at 1020 nm in summer, 0.70 (0.03) at 440 nm and 0.64 (0.05) at 1020 nm in autumn, and 0.70 (0.03) at 440 nm and 0.62 (0.06) at 1020 nm in winter. The largest ASY decrease is thus observed in winter, in line with the results reported by Alam *et al.* (2012) in Lahore and Karachi.

Aerosol Radiative Forcing

In this section, the values of ARF at the SURF and at the TOA over Évora during the period 2003–2015 are analyzed. Fig. 4 shows the values of DARF at the SURF and at the TOA obtained in Évora during the period 2003–2015 in a box and whisker plot. As can be seen, the DARF at the SURF shows some variability during the year, with more negative values in warm months and less negative values in cold months. DARF ranged from –0.1 to –54.9 W m^{-2}, with a mean (and standard deviation) of –7.4 (5.5) W m^{-2},

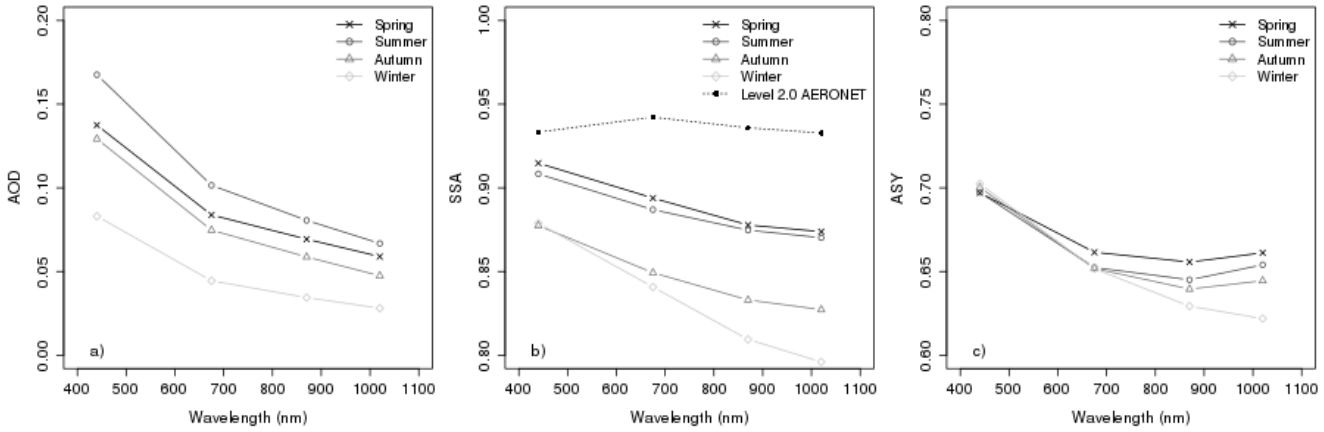

Fig. 3. (a), (b) and (c) show AOD, SSA and ASY mean values at wavelengths of 440 nm, 675 nm, 870 nm, and 1020 nm for different seasons. AERONET level 2.0 SSA has also been plotted in (b) for comparison purposes.

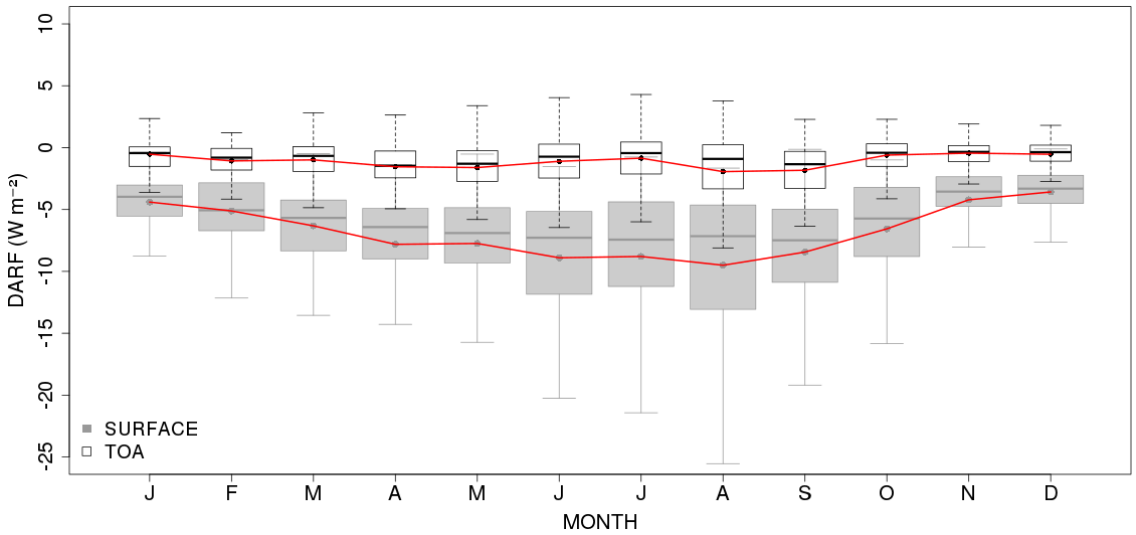

Fig. 4. Box and whisker plot of daily ARF values, DARF, at the surface and the top of the atmosphere for each calendar month over the 2003–2015 period. The mean (filled circles), median (horizontal segment within the box), 25th and 75th percentiles (top/bottom box limits) and data within 1.5 times the interquartile range (whiskers) are shown.

at the SURF, and from –15.6 to +18.9 W m^{-2}, with a mean value of –1.1 (2.5) W m^{-2}, at the TOA. The negative values indicate a decrease in the solar radiation reaching the SURF and an increase in the light scattered back to space at the TOA. This loss in net radiation at the TOA leads to cooling of the Earth–atmosphere system. It is worth mentioning that 491 DARF values are positive (29% of the total number of cases). These values are near zero, with 75% of cases below 1.3 W m^{-2}.

It is interesting to note that the absolute magnitude of the mean DARF at the SURF is higher than at the TOA, producing a mean net gain of energy by the atmosphere estimated in 6.3 (with a standard deviation of 4.8) W m^{-2}. This gain is due to the absorption of radiation by atmospheric components.

The monthly mean of this absorption by the atmosphere is represented by the difference between the two red lines in Fig. 4. These values ranged from 2.6 W m^{-2} in December to 7.1 W m^{-2} in August. These absorbing properties of aerosols are also particularly important for energy balance and cloud-aerosol interactions, as shown in the work of Su *et al.* (2008).

While no seasonal DARF pattern is observed at the TOA, a clear seasonal cycle is detected at the SURF (Fig. 4). This seasonality is not only due to the variation in the radiation along the year, but also to the seasonal pattern shown by AOD (Fig. 5(a)). This figure presents a box and whisker plot of daily AOD (at 550 nm) values over Évora for each calendar month, showing its annual variation. The lowest optical depths occur in November and December, contrasting with the highest optical depths found in August and September, when AOD is higher than 0.18 in more than 25% of the cases. These high AOD values during the summer months can be explained by a combination of several factors such as Saharan dust intrusions and forest fires, being the latter associated with high temperatures, very low atmospheric relative humidity and lack of precipitation. The arrival of air masses from the Saharan region transporting desert-dust aerosols constitutes a substantial source of aerosols, affecting the southwestern Iberian Peninsula generally in summer (Toledano *et al.*, 2007). This fact is confirmed by the low α values observed in August (Fig. 5(b)). Summer forest fires, particularly those extensive and long lasting that occurred in Portugal and Western Spain in 2003 and 2005 (Elias *et al.*, 2006), could mean also a substantial contribution to high optical depth values during these months. Both conditions (low AOD in winter months and high AOD values in summer months) are consistent with the ARF values shown in Fig. 4 (less negative in winter and more negative in summer). Also, a secondary maximum is observed in spring, being consistent with ARF values and observations reported for other stations of the Iberian Peninsula (Estellés *et al.*, 2007; Toledano *et al.*, 2007; Obregón *et al.*, 2012; Esteve *et al.*, 2014).

Fig. 5(b) depicts the annual variation of daily α, showing the highest mean values in January, December, February, and November. Conversely, α is low in April, May and August, being associated with large particles, typical of desert dust episodes or/and intrusions of marine aerosol in spring and summer (associated with sea breeze). In August, the low α values together with high AOD load, indicate the intrusion of dust from North Africa. Other studies have reported a similar seasonal pattern of AOD and α at other locations within the Iberian Peninsula, such as El Arenosillo (Cachorro *et al.*, 2005; Toledano *et al.*, 2007), Boecillo (Cachorro *et al.*, 2000), and Cáceres (Obregón *et al.*, 2015c). As it can be seen in Fig. 5(a), although AOD is high and similar in August and September, α differs between these two months. In August, α is lower than in September, indicating a stronger influence of desert dust aerosol in August than in September, and a higher cooling at the SURF. This tendency of cooling the Earth-atmosphere system due to the effect of desert dust aerosols agrees with results reported for other regions (e.g., Costa *et al.*, 2006; Derimian *et al.*, 2006;

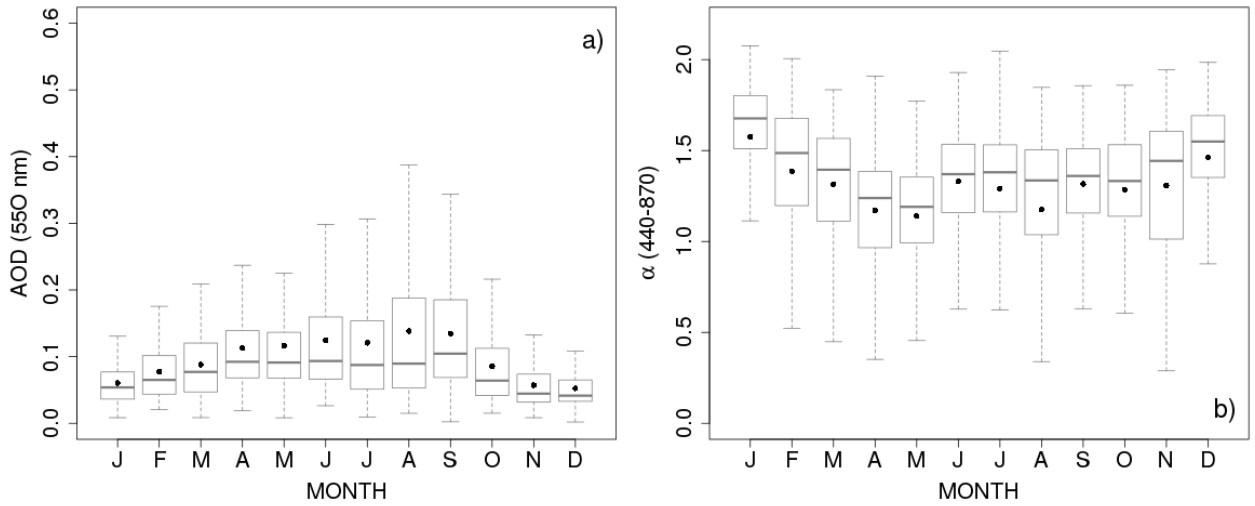

Fig. 5. Box and whisker plot of daily AOD (a) and α (b) values for each calendar month over the 2003–2015 period. The mean (filled circles), median (horizontal segment within the box), 25th and 75th percentiles (top/bottom box limits) and data within 1.5 times the interquartile range (whiskers) are shown.

Lyamani *et al.*, 2006; Cachorro *et al.*, 2008; Guerrero-Rascado *et al.*, 2009; Huang *et al.*, 2009; García *et al.*, 2012; Santos *et al.*, 2013; Valenzuela *et al.*, 2012; Obregón *et al.*, 2015a).

It is worth mentioning that our findings are not in line with results for the same station reported by Mateos *et al.* (2014) within a general study where several stations were analyzed. The monthly ARF values obtained here are generally more negative than theirs. In particular, the magnitude and the time of the year with the most negative ARF differ between both studies; while this study finds –9.5 W m^{-2} in August, they find around –8 W m^{-2} in April. One reason for this discrepancy could be related with the limited period of study considered by Mateos *et al.* (2014), which, for example, excluded the year 2003. During this year, as already mentioned above, there were numerous intense intrusions of desert dust and several forest fires all over Iberian Peninsula and south of France. The difference in ARF values emphasizes the need for relying on long term representative series of measurements in order to achieve an accurate estimation of the average regional aerosol radiative effect, mainly in areas with high variability such as the Iberian Peninsula.

An example of the spatial variability is the difference in ARF values reported for the Atlantic and the Mediterranean coastal areas within the Iberian Peninsula. Thus, the magnitude of the ARF obtained in this study at an Atlantic-influenced station such as Évora is around half the values measured at a Mediterranean station such as Burjassot (Valencia, Spain) (Esteve *et al.*, 2014). This difference is due to several factors such as the influence of the oceans, the prevailing circulation patterns and local aerosol sources. The results obtained in this study also show great differences with respect to those obtained in large polluted cities such as Lahore and Karachi in Pakistan. At these stations the ARF values are around –70 and –19 W m^{-2} at the SURF and at the TOA, respectively (Alam *et al.*, 2011; Alam *et al.*, 2014).

Fig. 6 shows comparisons between ARF at both levels SURF (a) and TOA (b), as provided by AERONET vs values estimated in this study using libRadtran. The comparisons are performed for the period of study. Values at the SURF show a good general agreement, with a high correlation coefficient of 0.97. This value is similar to those obtained by Alam *et al.* (2012) for Lahore and Karachi using SBDART model (0.99 and 0.98, respectively), and notably higher than those obtained by Bibi *et al.* (2017) over Karachi (0.51), Lahore (0.81), Jaipur (0.66) and Kanpur (0.69). This good correlation between AERONET and libRadtran surface forcing demonstrates that the input parameters, particularly the atmospheric profiles, constitute an appropriate representation of the prevailing atmospheric conditions in our location of study. On the other hand, the comparison between ARF at the TOA presents also a very high correlation coefficient (0.91) at the TOA (Fig. 6(b)). This value is notably higher than the values obtained by Bibi *et al.* (2017) over Karachi (0.46), Lahore (0.73), Jaipur (0.57) and Kanpur (0.55).

The libRadtran code allows to select two standard aerosol profiles, one typical of spring–summer and another of autumn–winter conditions. These profiles (Shettle, 1989) describe the change in the aerosol profile throughout the year. In order to analyze the sensitivity of the radiative forcing estimates to the vertical distribution of aerosols, these two profiles have been used. Thus, all the calculations have been repeated for both profiles separately regardless of the true season of the year and the daily aerosol radiative forcing has been obtained at the SURF and at the TOA. For the comparison analysis, the whole year 2012 has been used in order to account for the annual variability of the frequency of the aerosol conditions. The DARF estimated using both profiles show a very good agreement with a correlation coefficient near one. Differences in the DARF are very low at both levels, with mean differences of –0.001 Wm^{-2} (standard deviation of 0.009 Wm^{-2}) at the SURF, and of 0.012 Wm^{-2} (standard deviation of 0.050 Wm^{-2}) at the TOA. These results are in line with the sensitivity study

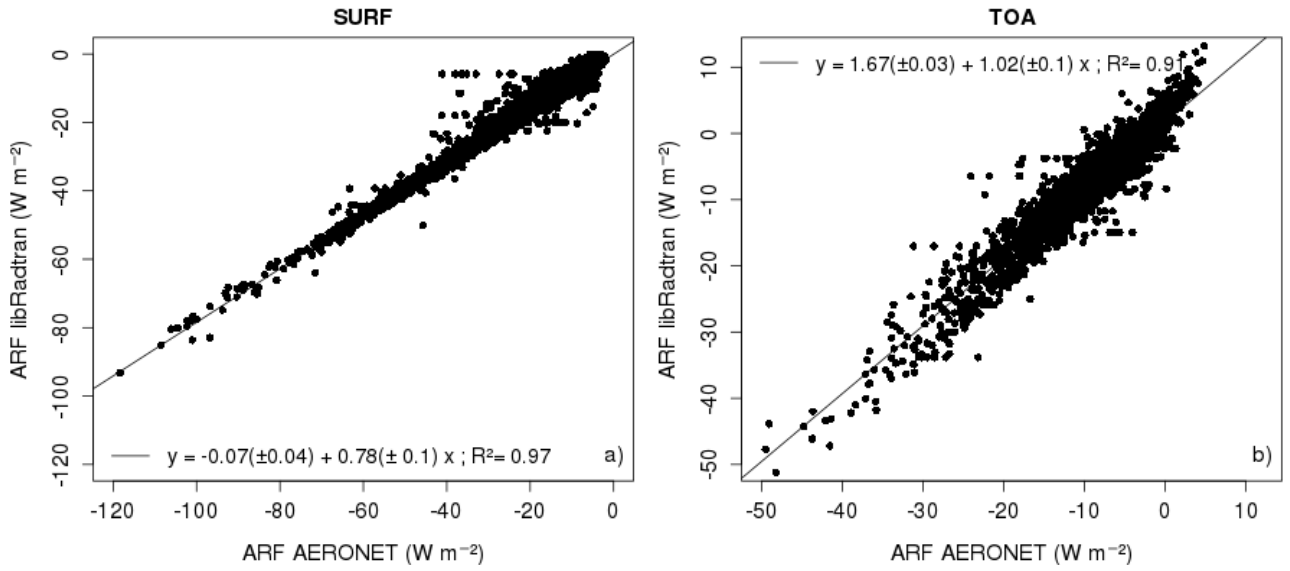

Fig. 6. Comparisons between ARF provided by AERONET and ARF estimated in this study using libRadtran, (a) for surface level and (b) for the top of the atmosphere level.

performed by Mishra *et al.* (2015), who concluded that aerosol forcing in the visible-near infrared range is less sensitive to changes in the aerosol layer height as compared to thermal-infrared and ultraviolet ranges.

As mentioned before, since the ARF depends on the particle load in the atmosphere, the forcing efficiency ARFE was calculated and analyzed at the SURF and at the TOA levels. The mean ARFE has been calculated as the slope of the regression line between ARF and AOD values. Since the ARF is expected to be zero when AOD is zero, a zero-intercept linear regression has been used to estimate the ARFE. Fig. 7 shows DARF at the SURF and at the TOA versus daily mean AOD (550 nm). The uncertainty in ARFE is quantified by the error associated to the regression slope. The ARFE obtained were –62.7 ± 0.4 W m^{-2} τ^{-1} and –14.3 ± 0.3 W m^{-2} τ^{-1} (per unit AOD or τ at 550 nm) for SURF and TOA datasets, respectively. In order to analyze the effect of SSA, in Fig. 7 the points have been colored according to their SSA value. As can be seen, for a given AOD, the most negative ARF values at the SURF correspond to low SSA values, i.e., to the most absorbing aerosols. Conversely, the opposite behavior is found at the TOA (Fig. 7(b)). Thus, the increase in the absorption by aerosols reduces the scattered radiation also towards TOA, thereby contributing to less negative (or even positive) ARF values at the TOA. These results are in line with those found during the CLEARCOLUMN/ACE2 campaign conducted at Sagres, Portugal (Silva *et al.*, 2002). They are also confirmed by the ARFE values calculated for different SSA intervals. Thus, the ARFE obtained for SURF were –140.2, –104.3, –81.4 and –55.48 W m^{-2} τ^{-1} for the SSA ranges [< 0.7], [0.7–0.8], [0.8–0.9], [>0 .9], respectively. Similarly, the following ARFE values: +44.5, +15.2, –3.4, –19.1 W m^{-2} τ^{-1}, were obtained for the TOA for the same SSA intervals mentioned above. While the aerosols at the SURF with low SSA result in highly negative ARFE values, at the TOA those aerosols are associated with less negative, or even positive, ARFE values.

The ARFE was also calculated at 500 nm in order to compare with the study performed by Esteve *et al.* (2014) for a Mediterranean station during the period 2003–2011. As mentioned before, notable differences exist between the Atlantic and the Mediterranean areas. Thus, while Évora shows –55.1 W m^{-2} τ^{-1} at the SURF and –15.1 W m^{-2} τ^{-1} at the TOA, Burjassot shows more negative values (–139 W m^{-2} τ^{-1} at the SURF and –19.2 W m^{-2} τ^{-1} at the TOA).

Fig. 8 shows the mean ARFE calculated for each season of the year at the SURF and at the TOA. Points have been colored according to their SSA value. No seasonal effect can be perceived at any level, with ARFE around –62 W m^{-2} τ^{-1} and –14 W m^{-2} τ^{-1} at the SURF and at the TOA, respectively. However, the aerosol tends to have a slightly stronger impact at the TOA in spring (–16.1 ± 0.7 W m^{-2} τ^{-1}) than in the remaining seasons: winter (–14.2 ± 0.9 W m^{-2} τ^{-1}), autumn (–13.9 ± 0.6 W m^{-2} τ^{-1}) and summer (–13.8 ± 0.4 W m^{-2} τ^{-1}).

Heating Rate

The amount of solar radiations trapped in the atmosphere by the aerosols as quantified by the atmospheric heating rate has been analyzed. The average heating rate (K day^{-1}) estimated from DARF during the study period was 0.18 (with a standard deviation of 0.15). Percentiles 10 and 90 indicate that in 80% of the days, HR falls between 0.04 and 0.35 K day^{-1}. These values are in line with the value of 0.11 K day^{-1} obtained by Valenzuela *et al.* (2017) for the same location (Évora) during one specific day. The heating rate in Évora is generally lower than values reported for stations with high atmospheric absorption such as, for example, two polluted mega-cities in Pakistan, with values higher than 1 K day^{-1} (Alam *et al.*, 2012). It is also lower than the values obtained for two desert dust events analyzed by Gharibzadeh *et al.* (2017), which showed mean values of 2.16 and 0.89 K day^{-1}.

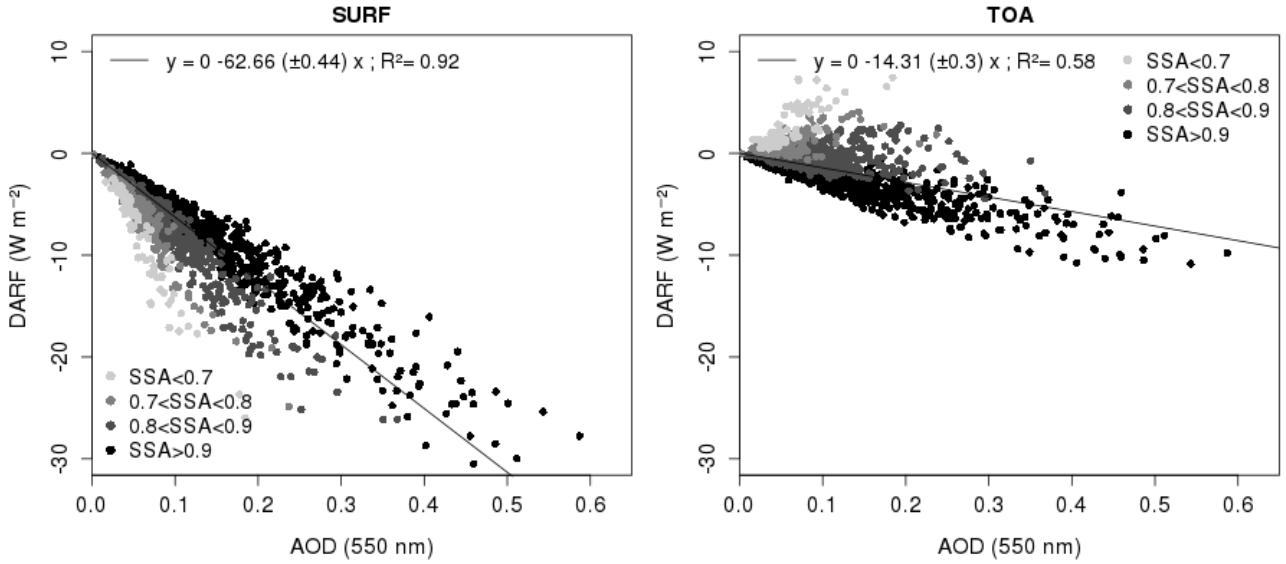

Fig. 7. Aerosol radiative forcing as a function of the AOD at 550 nm during the study period. (a) for surface level and (b) for the top of the atmosphere level. The regression equations are included and the points have been colored according to their SSA value.

In order to analyze the annual variation of the HR in Évora, the mean HR value was calculated for each calendar month (Fig. 9). The higher HR values occur mainly during summer (mean of 0.22 and standard deviation of 0.15), when ARF is also high. It is followed by spring (mean of 0.18 and standard deviation of 0.18), autumn (mean of 0.15 and standard deviation of 0.12) and winter (mean of 0.10 and standard deviation of 0.10). Spring is the season that shows the higher variability, with many high HR values during April. The annual variation in the amount of solar energy trapped by the atmosphere has strong implications for temperature changes and thermal structure of the atmosphere as well as important consequences for many processes, like cloud formation, precipitation, and synoptic circulation.

CONCLUSIONS

The aerosol radiative forcing (ARF) at Évora station has been studied with the goal of reducing the uncertainty of the aerosol impact at local scales. This station provides information about Southwestern Iberian Peninsula, a region of climatic significance largely affected by different aerosol types such as local continental particles, Atlantic marine aerosols, and desert dust coming from the largest source of dust worldwide: the Sahara Desert. Towards this aim, the aerosol radiative forcing and its efficiency (ARFE) in the shortwave solar spectrum have been calculated and analyzed. The study period extends from 2003 to 2015, being the longest period ever used in studies of aerosol radiative forcing in this region.

ARF and ARFE have been calculated at both the Earth's surface (SURF) and top of the atmosphere (TOA) levels. For this purpose, a high temporal resolution dataset, composed of 10-minute irradiance values simulated using the libRadtran code and previously validated, has been used. The ARF values calculated on a 10 minute basis have been integrated over 24 h to obtain daily mean values, DARF, for 1676 days. While no seasonal DARF pattern is observed at the TOA, a clear seasonal pattern can be distinguished at the SURF, with more negative values in summer, likely associated not only to the variation in the radiation along the year but also to the annual variability of AOD. The DARF values obtained for SURF ranged from –0.1 to –54.9 W m^{-2}, with a mean (and standard deviation) of –7.4 (5.5) W m^{-2}, and from –15.6 to +18.9 W m^{-2} at the TOA with a mean value of –1.1 (2.5) W m^{-2}. The negative values indicate a decrease in the solar radiation that reaches the Earth's surface and an increase in the light that is scattered back to space, cooling the Earth–atmosphere system. The difference in DARF magnitude between SURF and TOA indicates a mean net gain of energy by the atmosphere estimated in 6.3 (with a standard deviation of 4.8) W m^{-2}, due to absorption of radiation by atmospheric components.

The values of ARF at the SURF calculated in this study were compared with those reported by other authors for different regions, showing significant differences and indicating the importance to perform accurate local studies to achieve a thorough description of the impact of aerosols. The comparison with the study of Mateos *et al.* (2014) for the same station revealed notable differences, mainly in the ARF seasonal pattern. This discrepancy is likely associated to the use of a limited period of measurements in that study, emphasizing the need to use long high quality time series of data in order to guarantee an accurate description of the aerosol radiative forcing.

Instantaneous ARF values simulated with libRadtran have been compared with values provided by AERONET. The comparison showed a very good agreement at both levels: SURF and TOA, confirming the reliability of the calculations performed in this study with the libRadtran model.

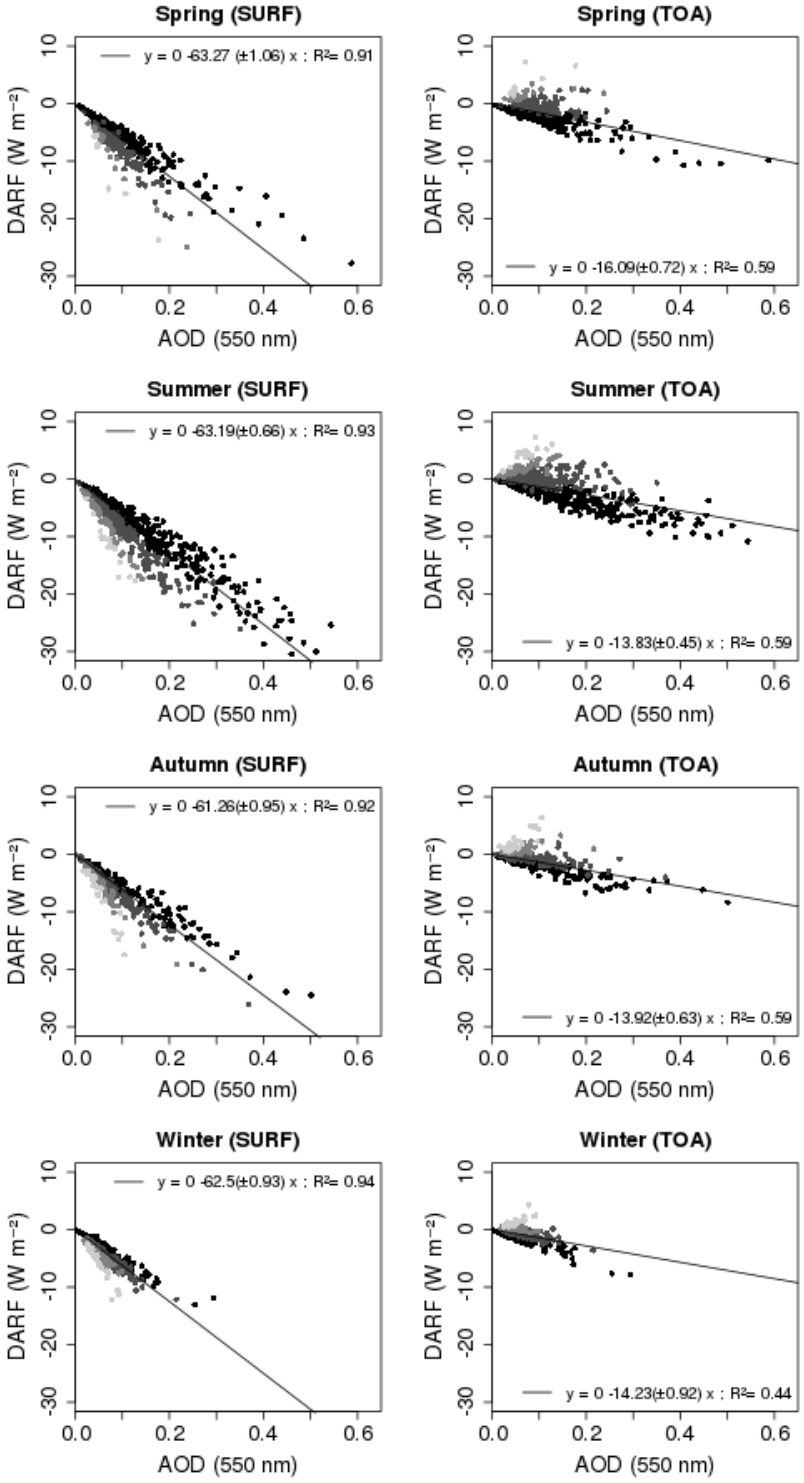

Fig. 8. Aerosol radiative forcing as a function of the AOD at 550 nm for each season of the year. The regression equations are included and the points have been colored according to their SSA value.

The ARFE (ARF per unit optical depth) was also calculated, and found to be –62.7 ± 0.4 W m^{-2} τ^{-1} and –14.3 ± 0.3 W m^{-2} τ^{-1} (per unit AOD or τ at 550 nm), at the SURF and at the TOA, respectively, showing no seasonality. These ARFE values are directly related to the SSA, with opposite behavior at the SURF and at the TOA. Thus, while at the SURF the aerosols with low SSA result in highly negative ARFE values, at the TOA those aerosols are associated with less negative or even positive ARFE values. This fact is due to the higher absorption by these aerosols, which results in less scattered radiation also towards the TOA and, therefore, in less negative ARFE at the TOA.

The values of ARF and ARFE reported for the region of study positively contributes to improve the understanding

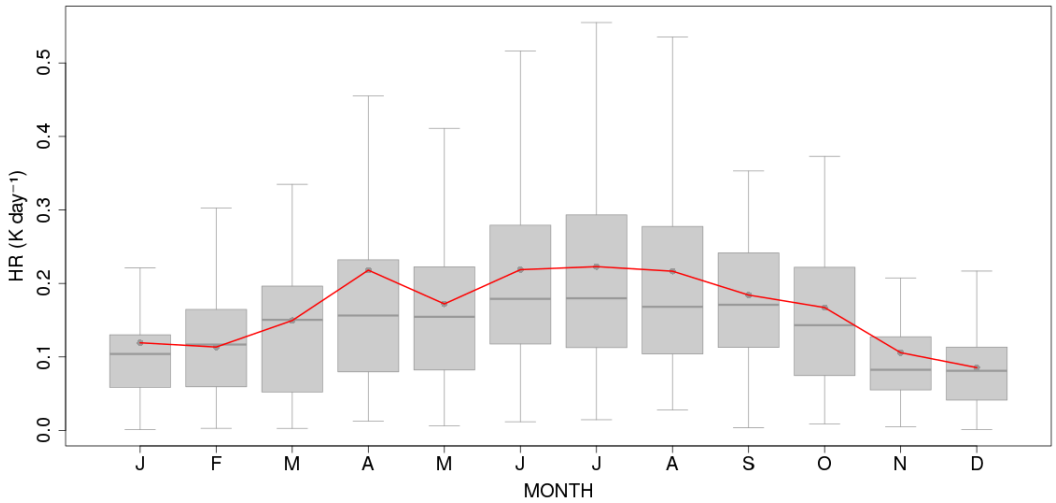

Fig. 9. Box and whisker plot of daily HR values for each calendar month over the 2003–2015 period. The mean (filled circles), median (horizontal segment within the box), 25th and 75th percentiles (top/bottom box limits) and data within 1.5 times the interquartile range (whiskers) are shown.

of the impact of aerosols in this area, mainly referred to its magnitude and temporal variability. In particular, the high temporal variability found in ARF and ARFE suggests the need to use long time series to guarantee the temporal representativeness in this interesting region.

ACKNOWLEDGMENTS

This work was partially supported by FCT (Fundação para a Ciência e a Tecnologia) through the grant SFRH/BPD/86498/2012. The work is co-funded by the European Union through the European Regional Development Fund, included in the COMPETE 2020 (Operational Program Competitiveness and Internationalization) through the ICT project (UID/GEO/04683/2013) with the reference POCI-01-0145-FEDER-007690 and also through the ALOP (ALT20-03-0145-FEDER-000004) and DNI-A (ALT20-03-0145-FEDER-000011) projects. The research is also co-funded by the research projects CGL2011-29921-C02-01/CLI and CGL2014-56255-C2-1-R granted by the "Ministerio de Economía y Competitividad" of Spain. The authors would like to acknowledge Samuel Bárias for maintaining instrumentation used in this work. Thanks are due to AERONET/PHOTONS and RIMA networks for the scientific and technical support. CIMEL calibration was performed at the AERONET-EUROPE GOA calibration center, supported by ACTRIS under agreement no. 654109 granted by European Union (H2020-INFRAIA-2014-2015). The data analyzed in this study are available from authors upon request (nines@unex.es).

REFERENCES

Alam, K., Trautmann, T. and Blaschke, T. (2011). Aerosol optical properties and radiative forcing over mega city Karachi. *Atmos. Res.* 101: 773–782.

Alam, K., Trautmann, T., Blaschke, T. and Majid, S. (2012). Aerosol optical and radiative properties during summer and winter seasons over Lahore and Karachi. *Atmos. Environ.* 50: 234–245.

Alam, K., Sahar, N. and Iqbal, Y. (2014). Aerosol characteristics and radiative forcing during pre-monsoon and post-monsoon in an urban environment. *Aerosol Air Qual. Res.* 14: 99–107.

Bibi, H., Alam, K., Blaschke, T., Bibi, S. and Iqbal, M.J. (2016). Long-term (2007-2013) analysis of aerosol optical properties over four locations in the Indo-Gangetic plains. *Appl. Opt.* 55: 6199–6211.

Bibi, H., Alam, K. and Bibi, S. (2017). Estimation of shortwave direct aerosol radiative forcing at four locations on the Indo-Gangetic Plains: Model results and ground measurement. *Atmos. Environ*. 163: 166–181.

Boucher, O. and Coauthors (2013). Clouds and aerosols in climate change 2013. In *Contribution of Working Group I to the Fifth Assessment Report of the Intergovernmental Panel on Climate Change*. Stocker, T.F., Qin, D., Plattner, G.K., Tignor, M., Allen, S.K., Boschung, J., Nauels, A., Xia, Y., Bex, V. and Midgley, P.M. (Eds.). The Physical Science Basis. Cambridge University Press, Cambridge, United Kingdom and New York, NY, USA.

Bush, B.C. and Valero, F.P.J. (2003). Surface aerosol radiative forcing at Gosan during the ACE-Asia campaign. *J. Geophys. Res.* 108: 1–8.

Cachorro, V.E., Durán, P., Vergaz, R. and Frutos, M.A. (2000). Measurement of the atmospheric turbidity of the North Centre continental area in Spain: Spectral aerosol optical depth and Ångström turbidity parameters. *J. Aerosol Sci*. 31: 687–702.

Cachorro, V.E., Toledano, C., de Frutos, A.M., Sorribas, M., Vilaplana, J.M. and de la Morena, B. (2005). Aerosol characterization at El Arenosillo (Huelva, Spain) with an AERONET/PHOTONS CIMEL sunphotometer. *Geophys. Res. Abstr.* 7: 08559.

Cachorro, V.E., Toledano, C., Prats, N., Sorribas, M., Mogo, S., Berjón, A., Torres, B., Rodrigo, R., de la Rosa, J. and De Frutos, A.M. (2008). The strongest desert dust intrusion

mixed with smoke over the Iberian Peninsula registered with Sun photometry. *J. Geophys. Res*. 113: D14S04.

Costa, M.J., Sohn, B.J., Levizzani, V. and Silva, A.M. (2006). Radiative forcing of Asian dust determined from the synergized GOME and GMS satellite data – A case study. *J. Meteorol. Soc. Jpn*. 84: 85–95.

Derimian, Y., Karnieli, A., Kaufman, Y.J., Andreae, M.O., Andreae, T.W., Dubovik, O., Maenhaut, W., Koren, I. and Holben, B.N. (2006). Dust and pollution aerosols over the Negev desert, Israel: Properties, transport, and radiative effect. *J. Geophys. Res*. 111: D05205.

Di Biagio, C., di Sarra, A. and Meloni, D. (2010). Large atmospheric shortwave radiative forcing by Mediterranean aerosols derived from simultaneous ground-based and spaceborne observations and dependence on the aerosol type and single scattering albedo. *J. Geophys. Res*. 115: D10209.

Dubovik, O., Holben, B., Eck, T.F., Smirnov, A., Kaufman, Y.J., King, M.D., Tanré, D. and Slutsker, I. (2002). Variability of absorption and optical properties of key aerosol types observed in worldwide locations. *J. Atmos. Sci.* 59: 590–608.

Eck, T.F., Holben, B.N., Reid, J.S., Dubovik, A., Smirnov, N.T.O'Neill,, Slutsker, I. and Kinne, S. (1999). Wavelength dependence of the optical depth of biomass burning, urban, and desert dust aerosols. *J. Geophys. Res.* 104: 00093–00095.

Elias, T., Silva, A.M., Belo, N., Pereira, S., Formenti, P., Helas, G. and Wagner, F. (2006). Aerosol extinction in a remote continental region of the Iberian Peninsula during summer. *J. Geophys. Res*. 111: 1–20.

Emde, C., Buras-Schnell, R., Kylling, A., Mayer, B., Gasteiger, J., Hamann, U., Kylling, J., Richter, B., Pause, C., Dowling, T., Bugliaro, L. (2016). The libRadtran software package for radiative transfer calculations (version 2.0.1). *Geosci. Model Dev.* 9: 1647–1672.

Escudero, M., Castillo, S., Querol, X., Avila, A., Alarcón, M., Viana, M.M., Alastuey, A., Cuevas, E. and Rodríguez, S. (2005). Wet and dry African dust events over eastern Spain. *J. Geophys. Res*. 110: D18S08.

Estellés, V., Martínez-Lozano, J.A., Utrillas, M.P. and Campanelli, M. (2007). Columnar aerosol properties in Valencia (Spain) by ground based sun photometry. *J. Geophys. Res*. 112: D11201.

Esteve, A.R., Estellés, V., Utrillas, M.P. and Martínez-Lozano, J.A. (2014). Analysis of the aerosol radiative forcing over a Mediterranean urban coastal site. *Atmos. Res*. 137: 195–204.

Foyo-Moreno, I., Alados, I., Antón, M., Fernández-Gálvez, J., Cazorla, A. and Alados-Arboledas, L. (2014). Estimating aerosol characteristics from solar irradiance measurements at an urban location in southeastern Spain. *J. Geophys. Res.* 119: 1845–1859.

García, O.E., Díaz, J.P., Expósito, F.J., Díaz, A.M., Dubovik, O., Derimian, Y., Dubuisson, P. and Roger, J.C. (2012). Shortwave radiative forcing and efficiency of key aerosol types using AERONET data. *Atmos. Chem. Phys*. 12: 5129–5145.

Gharibzadeh, M., Alam, K., Bidokhti, A.A., Abedini, Y. and Masoumi, A. (2017). Radiative effects and optical properties of aerosol during two dust events in 2013 over Zanjan, Iran. *Aerosol Air Qual. Res.* 17: 888–898.

Guerrero-Rascado, J.L., Olmo, F.J., Avilés-Rodríguez, I., Navas-Guzmán, F., Pérez-Ramírez, D., Lyamani, H. and Alados Arboledas, L. (2009). Extreme Saharan dust event over the southern Iberian Peninsula in september 2007: Active and passive remote sensing from surface and satellite. *Atmos. Chem. Phys*. 9: 8453–8469.

Gueymard, C. (2004). The sun's total and spectral irradiance for solar energy applications and solar radiation models. *Sol. Energy* 76: 423–453.

Hansen, J., Sato, M., Kharecha, P. and von Schuckmann, K. (2011). Earth's energy imbalance and implications. *Atmos. Chem. Phys*. 11: 13421–13449.

Holben, B., Eck, T.F., Slutsker, I., Tanre, D., Buis, J., Setzer, K., Vermote, E., Reagan, J., Kaufman, Y., Nakajima, T., Lavenu, F., Jankowiak, I. and Smirnov, A. (1998). AERONET—A federated instrument network and data archive for aerosol characterization. *Remote Sens. Environ*. 66: 1–16.

Holben, B.N., Eck, T.F., Slutsker, I., Smirnov, A., Sinyuk, A., Schafer, J., Giles, D. and Dubovik, O. (2006). Aeronet's Version 2.0 quality assurance criteria, Proc. SPIE 6408, *Remote Sensing of the Atmosphere and Clouds*, 64080Q (8 December 2006).

Huang, J., Fu, Q., Su, J., Tang, Q., Minis, P., Hu, Y., Yi, Y. and Zhao, Q. (2009). Taklimakan dust aerosol radiative heating derived from CALIPSO observations using the Fu–Liou radiation model with CERES constraints. *Atmos. Chem. Phys*. 9: 4011–4021.

Kaskaoutis, D., Sinha, P., Vinoj, V., Kosmopoulos, P., Tripathi, S., Misra, A., Sharma, M. and Singh, R. (2013). Aerosol properties and radiative forcing over Kanpur during severe aerosol loading conditions. *Atmos. Environ.* 79: 7–19.

Koppen, W. (1936). Das geographisca System der Klimate, In *Handbuch der Klimatologie*, Koppen, W. and Geiger, G. (Eds.), 1. C. Gebr, Borntraeger, pp. 1–44.

Liou, K.N. (2002). *An Introduction to Atmospheric Radiation*. Academic press.

Lyamani, H., Olmo, F.J., Alcántara, A and Alados-Arboledas, L. (2006). Atmospheric aerosols during the 2003 heat wave in southeastern Spain II: Microphysical columnar properties and radiative forcing. *Atmos. Environ*. 40: 6465–6476.

Mateos, D., Antón, M., Toledano, C., Cachorro, V.E., Alados-Arboledas, L., Sorribas, M., Costa, M.J. and Baldasano, J.M. (2014). Aerosol radiative effects in the ultraviolet, visible, and near-infrared spectral ranges using long-term aerosol data series over the Iberian Peninsula. *Atmos. Chem. Phys*. 14: 13497–13514.

Mayer, B. and Kylling, A. (2005). Technical note: The libRadtran software package for radiative transfer calculations — description and examples of use. *Atmos. Chem. Phys*. 5: 1855–1877.

Mishra, A.K., Koren, I. and Rudich, Y. (2015). Effect of aerosol vertical distribution on aerosol-radiation interaction: A theoretical prospect. *Heliyon* 1: e00036.

Obregón, M.A., Pereira, S., Wagner, F., Serrano, A., Cancillo, M.L. and Silva, A.M. (2012). Regional differences of column aerosol parameters in western Iberian Peninsula. *Atmos. Environ*. 12: 1–10.

Obregón, M.A., Pereira, S., Salgueiro, V., Costa, M.J., Silva, A.M., Serrano, A. and Bortoli, D. (2015a). Aerosol radiative effects during two desert dust events in August 2012 over the Southwestern Iberian Peninsula. *Atmos. Res*. 153: 404–415.

Obregón, M.A., Serrano, A., Costa, M.J. and Silva, A.M. (2015b). Validation of libRadtran and SBDART models under different aerosol conditions. *IOP Conf. Series: Earth and Environmental Science.* 28: 012010.

Obregón, M.A., Serrano, A., Cancillo, M.L., Cachorro, V.E. and Toledano, C. (2015c). Aerosol radiometric properties at Western Spain (Cáceres station). *Int. J. Climatol*. 35: 981–990.

Pereira, S., Silva, A.M., Elias, T. and Wagner, F. (2005). Aerosol monitoring at Cabo da Roca site. Paper presented at *4° Simpósio de Meteorologia e Geofísica da APMG/6° Encontro Luso-Espanhol de Meteorologia*, Sesimbra, Portugal.

Pereira, S., Wagner, F. and Silva, A.M. (2008). Scattering properties and mass concentration of local and long-range transported aerosols over the South Western Iberia Peninsula. *Atmos. Environ*. 42: 7623–7631.

Pereira, S.N., Wagner, F. and Silva, A.M. (2011). Seven years of measurements of aerosol scattering properties, near the surface, in the south-western Iberia Peninsula. *Atmos. Chem. Phys*. 11: 17–29.

Querol, X., Rodriguez, S., Cuevas, E., Viana, M.M. and Alastuey, A. (2002). Intrusiones de masas de aire africano sobre la Península Ibérica y Canarias: Mecanismos de transporte y variación estacional. *3rd Asamblea Hispano portuguesa de Geodesia y Geofísica*. Inst. Nac. de Meteorol. Esp., Valencia.

Rodriguez, S., Querol, X., Alastuey, A., Kallos, G. and Kakaliagou, O. (2001). Saharan dust contributions to PM_{10} and TSP levels in Southern and Eastern Spain. *Atmos. Environ.* 35: 2433–2447.

Román, R., Bilbao, J. and de Miguel, A. (2014). Solar radiation simulations in the Iberian Peninsula: Accuracy and sensitivity to uncertainties in inputs of a radiative transfer model. *J. Quant. Spectrosc. Radiat.* 145: 95–109.

Salgueiro, V., Costa, M.J., Silva, A.M. and Bortoli., D. (2014). Variability of the daily-mean shortwave cloud radiative forcing at the surface at a midlatitude site in Southwestern Europe. *J. Clim.* 27: 7769–7780.

Santos, D., Costa, M.J. and Silva, A.M. (2008). Direct SW aerosol radiative forcing over Portugal. *Atmos. Chem. Phys*. 8: 5771–5786.

Santos, D., Costa, M.J., Silva, A.M. and Salgado, R. (2013). Modeling Saharan desert dust radiative effects on clouds. *Atmos. Res*. 127: 178–194.

Shettle, E. (1989). Models of aerosols, clouds and precipitation for atmospheric propagation studies, atmospheric propagation in the UV, visible, IR and mm-region and related system aspects. In 454 *in AGARD Conference Proceedings*.

Silva, A.M., Von Hoyningen-Huene, W., Bugalho, L., Schmidt, T., Costa, M.J. and Heintzenberg, J. (2002). Aerosol optical properties from columnar data during the second Aerosol Characterization Experiment on the south coast of Portugal. *J. Geophys. Res.* 107: 4642.

Silva, A.M., Costa, M.J., Elias, T., Formenti, P., Belo, N. And Pereira, S. (2003). Ground-based aerosol monitoring at Évora, Portugal. *Global Change News Lett*. 56: 6–10.

Silva, A.M., Wagner, F., Pereira, S. and Elias, T. (2006). Aerosol properties at the most western point of continental Europe. *Paper presented at International Aerosol Conference*, Minnesota, USA.

Singh, A., Tiwari, S., Sharma, D., Singh, D., Tiwari, S., Srivastava, A.K., Rastogi, N. and Singh, A. (2016). Characterization and radiative impact of dust aerosols over northwestern part of India: A case study during a severe dust storm. *Meteorol. Atmos. Phys*. 128: 779–792.

Singh, S., Soni, K., Bano, T., Tanwar, R., Nath, S. and Arya, B. (2010). Clear-sky direct aerosol radiative forcing variations over mega-city Delhi. *Ann. Geophys*. 28: 1157–1166.

Stamnes, K., Tsay, S.C., Wiscombe, W. and Laszlo, I. (2000). DISORT, a general purpose Fortran program for discrete-ordinate-method radiative transfer in scattering and emitting layered media: Documentation of methodology. *Goddard Space Flight Center*, NASA.

Su, J., Huang, J., Fu, Q., Minnis, P., Ge, J. and Bi, J. (2008). Estimation of Asian dust aerosol effect on cloud radiation forcing using Fu-Liou radiative model and CERES measurements. *Atmos. Chem. Phys.* 8: 2763–2771.

Toledano, C. (2005). Climatología de los aerosoles mediante la caracterización de propiedades ópticas y masas de aire en la estación El Arenosillo de la red AERONET (PhD thesis) *Universidad de Valladolid*, Spain.

Toledano, C. (2006). Field calibration methods for aerosol optical depth determination with sun photometers. *Opt. Pura Apl*. 39: 303–311.

Toledano, C., Cachorro, V.E., de Frutos, A.M., Sorribas, M., Prats, N. and de la Morena, B. (2007). Inventory of African desert dust events over the southwestern Iberian Peninsula in 2000–2005 with an AERONET CIMEL Sun photometer. *J. Geophys. Res*. 112: D21201.

Valenzuela, A., Olmo, F.J., Lyamani, H., Antón, M., Quirantes, A and Alados-Arboledas, L. (2012). Aerosol radiative forcing during African desert dust events (2005–2010) over Southeastern Spain. *Atmos. Chem. Phys*. 12: 10331–10351.

Valenzuela, A., Costa, M.J., Guerrero-Rascado, J.L., Bortoli, D. and Olmo, F.J. (2017). Solar and thermal radiative effects during the 2011 extreme desert dust episode over Portugal. *Atmos. Environ*. 148: 16–29.

Received for review, May 3, 2017
Revised, September 5, 2017
Accepted, September 8, 2017